SYSTEMS SCIENCE & CONTROL ENGINEERING: AN OPEN ACCESS JOURNAL
2024, VOL. 12, NO. 1, 2438866
https://doi.org/10.1080/21642583.2024.2438866



# Event-triggered boost converter model predictive control with Kalman filter*

Ranya Badawi and Jun Chen

Department of Electrical and Computer Engineering, Oakland University, Rochester, MI, USA

**ABSTRACT**

Event-triggered control has been gaining popularity as a method to reduce the computational burden of model predictive control (MPC). Existing literature reports its successful use in power converter applications. In our survey, event-triggered model predictive control (ET-MPC) is used to improve the computational performance of an enumeration-based MPC controlled boost converter. ET-MPC solves an optimal control problem (OCP) to generate an optimal actuating value only when an event is triggered as opposed to solving the OCP at every time step, and hence reduce the computational load. In addition, a Kalman Filter-based estimator is added to the control system to ensure accurate voltage tracking even in the presence of model mismatch, which commonly occurs during load transients. The novelty of this work lies in the selection of the actuating control signal, where the control actions are selected from the optimal switching sequence as opposed to upholding the last value of the optimal actuating value as reported in prior literature. Extensive simulation evaluations are conducted to compare the performance of conventional time-triggered MPC and the proposed event-triggered MPC, where the event-trigger threshold is used as a tuning parameter to balance computation and control performance.

**ARTICLE HISTORY**
Received 4 July 2024
Accepted 27 November 2024

**KEYWORDS**
Model predictive control; MPC; event-trigger control; optimization control problem; Kalman filter; boost converter

## 1. Introduction

MPC has been gaining popularity as a control method for power converters (Ahmed et al., 2020a, 2020b; Han et al., 2021; Rodriguez & Cortes, 2012; Serri & Ahmad, 2016). MPC is an intuitive control method which utilizes a system model and a control objective to select an optimal actuating control signal. This is achieved by solving a cost function which generates an optimal control sequence across a prediction horizon (Rawlings et al., 2017). Traditional MPC utilizes a receding horizon approach in which the first control signal in the optimal control sequence is selected at each time step the OCP is triggered. The rest of the sequence is dismissed, and a new one is generated at the following time step. The predictive nature of the controller enables a faster system response. Another advantage of the MPC controller is that it can handle multiple inputs and outputs since it captures their interactions through the system model. Additionally, the inclusion of control objectives and protections within the cost function allows the system designer to reduce the number of sensors (Chen, Behal, et al., 2021; Chen, Li, et al., 2021; Chen, Liang, et al., 2021; Liang et al., 2019; Umeno & Maruta, 2020; Xie et al., 2009). Recent advancements in the processing speed of modern microcontrollers has allowed for a wider use of MPC in power converter control.

The control objective of a DC-DC boost converter is to have the output voltage track a reference voltage. Regulation must be achieved despite disturbances on the input voltage and load variations. Additional control objectives can be included such as current limiting to protect components from overheating and to protect magnetic devices from reaching saturation. Another control objective is limiting the switching frequency to reduce switching losses.

A brief explanation of a time-triggered enumeration-based MPC controller for a boost converter is shown in Figure 1. It starts with a math model of the converter. The model receives a set of switching sequences that span across the selected prediction horizon. The prediction horizon duration is equal to the number of switching states $N$ multiplied by the time step $T_s$. The model solves the OCP using the switching sequences along with the inductor current and output voltage measurements to

**CONTACT** Jun Chen junchen@oakland.edu

*Some preliminary results were presented at *2022 European Control Conference* (Badawi & Chen, 2022a) and *2022 IEEE Vehicle Power and Propulsion Conference* (Badawi & Chen, 2022b). This paper extends the conference versions by adding a Kalman Filter-based state and disturbance estimator, enhancing the controller by utilizing the inductor current measurement for current limiting, and providing a substantially more detailed description of the implementation of the proposed event-triggered model predictive control.

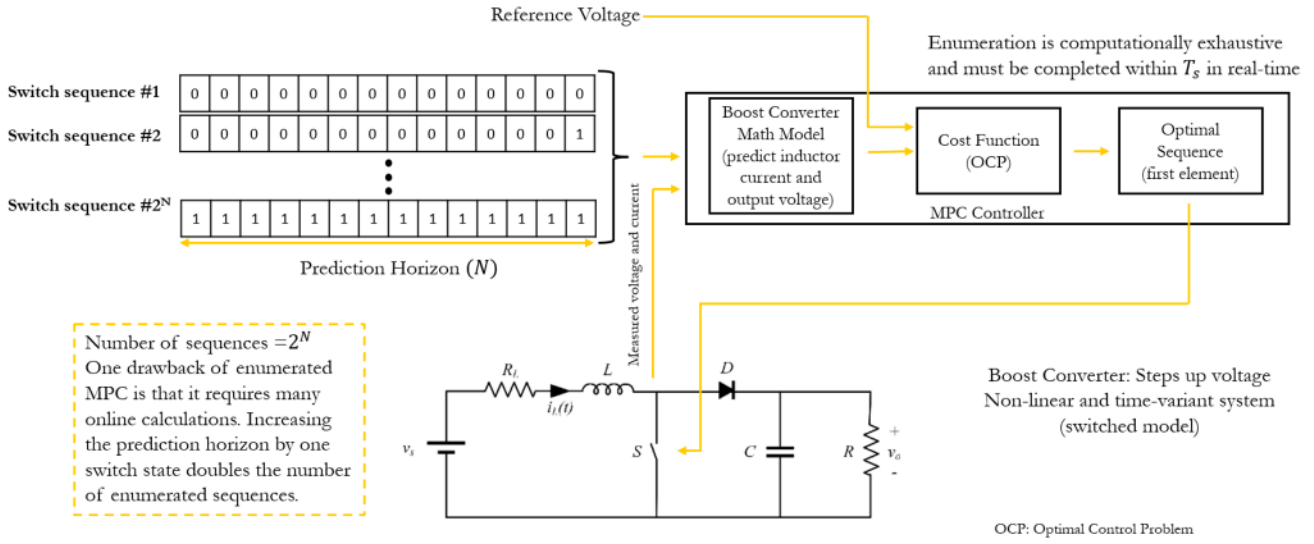


**Figure 1.** Enumeration-based model predictive control for boost converter.

decide which sequence achieves voltage regulation while meeting other system objectives.

Model inaccuracies are introduced as the time step ($T_S$) increases and due to parameter tolerances. These inaccuracies will not allow the controller to regulate the voltage effectively. Another example is during a load transient where the load resistance used in the model changes. The regulation performance of the time-triggered MPC boost converter during load transients can be improved through the implementation of a Kalman Filter-based disturbance observer (Beccuti et al., 2009; Hargrave, 1989; Karamanakos et al., 2013; Pannocchia, 2015; Pannocchia & Bemporad, 2007; Rigatos et al., 2018) which is described in a later section.

The purpose of this work is to develop an event-triggered MPC to reduce the computational burden of enumeration-based direct MPC in the control of a boost converter. It has been shown in Badawi and Chen (2022a, 2022b) that significant computational savings can be realized as the event-trigger threshold increases while comparable performance to an enumeration-based MPC can be accomplished. However, a trade-off must be made while selecting the trigger threshold to reduce the tracking error, voltage ripple and inductor peak current during steady state operation. We show in this work that during certain operating conditions, an 85% reduction in computations can be achieved. Additionally, a Kalman filter-based disturbance observer is introduced to address load transients, which is used to estimate the state variable and disturbances and compensate for the error introduced into the model due to the change in load. The results shared in Section 7 demonstrate that the event-triggered MPC is effective in reducing the computational burden during a load transient while reducing the settling time up to 1 ms during the transient.

The rest of this paper is organized as follows. A literature review of relevant work is presented in Section 2. Section 3 gives an overview of the discrete-time model of a DC-DC boost converter and the Kalman-based estimator. Section 4 describes the implementation of the proposed event-triggered MPC for a boost converter. Simulation results highlighting the performance of the event-triggered controller under different operating conditions including reference voltage changes and load transients using a Kalman-based disturbance estimator are presented in Section 5. We discuss the influence of the control parameters in Section 6 and the paper is concluded in Section 7 with future work directions.

## 2. Literature review

Power converters which utilize MPC in their control can be generally categorized as direct MPC or indirect MPC (Karamanakos & Geyer, 2020). Direct MPC is when the output of the controller directly actuates the switch and it has been implemented in Kouro et al. (2008), Karamanakos et al. (2013), Villarroel et al. (2021) and Snehal et al. (2021). Indirect control MPC implements a modulator which receives an optimal duty cycle from the controller and has been implemented in Jin et al. (2022), Geyer et al. (2008), Beccuti et al. (2009), L. Chen et al. (2019) and Liang et al. (2018). Direct control is particularly challenging due to the processing of a large amount of computations in a short sampling interval. Direct MPC with reference tracking is also known as Finite Control Set (FCS) since it utilizes a finite number of possible switch positions to

define the switching sequences (Cortes et al., 2009; Di Salvo et al., 2022; Ding et al., 2022; Gardezi & Hasan, 2018; Karamanakos & Geyer, 2020). One major drawback of FCS MPC is its extensive need for computational resources as a large number of computations are conducted within a sampling period on the order of microseconds. Due to this challenge, FSC MPC comes with a risk of being computationally intractable (Karamanakos et al., 2020). The computational burden is especially an issue for converters with non-minimum phase behaviour such as boost and buck-boost converters. Non-minimum phase behaviour in a boost converter translates to an initial delay in the response of the converter when the main switch is set to the *ON* position. This results in a slight dip in the output voltage, which then adjusts after several switching cycles. In an enumeration based MPC control scheme, this response requires an extension of the switching sequence prediction horizon $NT_s$.

Implementing an event-triggered MPC (ET-MPC) method saves on computational resources and has been implemented in different applications and referenced in Eqtami et al. (2011), J. Chen et al. (2022), Chen and Yi (2021), Yoo and Johansson (2021), Li and Shi (2014) and Hashimoto et al. (2016) and on a boost converter in Badawi and Chen (2022a, 2022b). The results show significant computational savings with comparable performance to the time-triggered formulation. In Chen, Wang, et al. (2021), event-trigger control applied to a FCS MPC is used to regulate the voltage of a three-phase inverter. When the voltage is within the set criteria, the control action is held, but if the criteria are not met, the MPC algorithm is run and a new action is calculated and applied. Since the use of event-trigger reduced the control signal (switching) variation, it allowed for the removal of the switching penalty from the cost function.

ET-MPC was utilized to control a buck converter in Wang et al. (2020) and Rathore and Fulwani (2016). The work in Wang et al. (2020) developed a method to design the event trigger condition and removed the switching criteria from the cost function. The results show a reduction in overall computational burden and switching losses. A similar technique was also implemented in Liang et al. (2023) to control a current-source-mode single-inductor multiple-output (CSM-SIMO) buck converter to minimize cross-regulation across the different outputs and reduce the overall computational burden of FCS-MPC. In Lin et al. (2021), ET-MPC is applied to the power control loop of a three-phase two-level grid-connected power converter to control active and reactive power. The work in Liu et al. (2022) furthers the ET-MPC mechanism by applying an extended state observer to address math model uncertainties for a modular multilevel converter.

Compared to these literature, the contribution of our work is the introduction of the event-triggered mechanism to a time-triggered enumeration based MPC in which the actuation signals are selected from the optimal switching sequence. An event is triggered when the measured (or estimated) output voltage deviates beyond the value in the optimal state trajectory based on the set trigger-threshold. An event can also be triggered if the consecutive control steps exceed the secondary prediction horizon which we later define as $k_{\max}$. Once an event is triggered, the MPC controller will run and generate a new optimal switch sequence and state trajectory. The actuation signals are initially predicted across the prediction horizon using a move blocking scheme. The optimal control sequence and state signals are cycled through the controller and reused. What distinguishes our work from previous work is the use of the actuation signals from the optimal control sequence rather than holding up the last value when an event is not triggered. The measured (estimated) output voltage is then compared to the corresponding projected state variable. If the deviation exceeds the trigger threshold, then another event is triggered and a new sequence is generated. We also apply a limit to the allowable number of elements in the optimal state sequence that can be applied. Previous work, Wang et al. (2020), Rathore and Fulwani (2016), Liang et al. (2023), Lin et al. (2021) and Liu et al. (2022) only upholds the last actuation value until the output voltage deviates from the reference voltage beyond a trigger-threshold. A more detailed explanation or our method is presented in a later section along with an evaluation of the impact of the trigger-threshold on the converter's performance. This work furthers our results which were originally reported in Badawi and Chen (2022a, 2022b) by adding a Kalman Filter-based state and disturbance estimator. We also provide further enhancements to the controller by utilizing the inductor current measurement for current limiting. Additionally, we provide a more detailed description of the implementation of an ET-MPC for power converters.

## 3. Mathematical model

MPC requires an accurate model of the system to predict the optimal actuation signal every time step, $T_s$. Switched-mode power converters are time-variant and non-linear systems, and the modelling of such systems can be done in multiple ways. One common approach in Pulse-Width Modulation (PWM) converter control is to create an AC equivalent circuit model by averaging the inductor voltage and capacitor current waveforms over a single switch cycle. Small AC variations around a quiescent operating point are then introduced into the model and the system

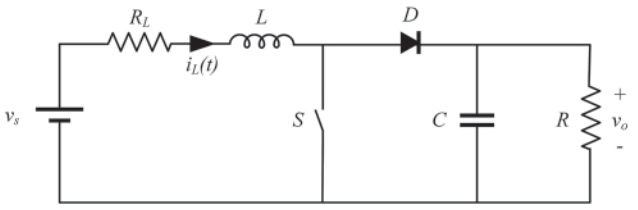


**Figure 2.** Boost converter circuit diagram.

is then linearized by removing second order AC (nonlinear) terms (Erickson & Maksimovic, 2007).

In PWM converter control, the output of the controller (or compensator) is a control voltage that is sent to a modulator. The modulator then translates the voltage to a duty cycle to actuate one or more switches at a fixed frequency. The duty cycle regulates the output voltage according to the system's transfer function. In Direct MPC, the output of the controller is directly manipulating the main switch $S$ of the boost converter in Figure 2, where the switching frequency varies. Without imposing a restriction to the switching frequency or amount of switching within the cost function, the frequency of the converter can reach up to $1/(2T_s)$ (Karamanakos et al., 2013). Due to the discrete nature of the boost converter (Cortes et al., 2009), which depends on switch $S$ position and inductor current, a hybrid model similar to Karamanakos et al. (2013) can be constructed and used to develop a math model.

### 3.1. Discrete-time model

The forward Euler approximation is used to derive a discrete-time model from the continuous-time model in Karamanakos et al. (2013) and Badawi and Chen (2022a) where the time increment is defined by $T_s$. The state variable is defined in (1), where $i_L$ is the inductor current and $v_o$ is the output voltage (capacitor voltage).

$$x[k] = \begin{bmatrix} i_L[k] & v_o[k] \end{bmatrix}^T \tag{1}$$

The boost converter operates in four distinct modes depending on the switch state and magnitude of the inductor current. The first mode is when the switch $S$ is *ON* and inductor current is positive and increasing. In this mode, the diode $D$ is *OFF*, and the output is supported by the capacitor. The second mode is when the switch is *OFF*. In this case, the inductor will induce a voltage that will force the current to continue flowing in the same direction through the diode to the load. The third mode occurs when the switch is *OFF* and the inductor current is decreasing and reaches zero, in this case, the diode is also *OFF*. The instance the inductor current reaches 0 is defined by $\tau_1$. During the fourth mode the switch remains in the *OFF* position and inductor current remains zero for the entire time step $T_s$ (Karamanakos et al., 2013).

The discrete-time state space matrices for all four modes are included below (2a).

Mode 1 (2a):

$$x[k+1] = \begin{bmatrix} 1 - \frac{R_L T_s}{L} & 0 \\ 0 & 1 - \frac{T_s}{RC} \end{bmatrix} x[k] + \begin{bmatrix} \frac{T_s}{L} \\ 0 \end{bmatrix} v_s[k] \tag{2a}$$

Mode 2 (2b):

$$x[k+1] = \begin{bmatrix} 1 - \frac{R_L T_s}{L} & -\frac{T_s}{L} \\ \frac{T_s}{C} & 1 - \frac{T_s}{RC} \end{bmatrix} x[k] + \begin{bmatrix} \frac{T_s}{L} \\ 0 \end{bmatrix} v_s[k] \tag{2b}$$

Mode 3 (2c):

$$\begin{bmatrix} 1 - \frac{R_L \tau_1}{L} & -\frac{\tau_1}{L} \\ \frac{\tau_1}{C} & 1 - \frac{T_s}{RC} \end{bmatrix} x[k] + \begin{bmatrix} \frac{\tau_1}{L} \\ 0 \end{bmatrix} v_s[k] \tag{2c}$$

Mode 4 (2d):

$$\begin{bmatrix} 1 & 0 \\ 0 & 1 - \frac{T_s}{RC} \end{bmatrix} x[k] \tag{2d}$$

### 3.2. Kalman filter implementation

An accurate measurement of the state variables is required to achieve robust control using MPC. This can be achieved through a state estimator. State estimators can be divided into deterministic (such as the Luenberger Filter) and Stochastic (e.g. Kalman Filter) state estimators. Nonlinear state estimators exist such as Particle Filters, Extended Kalman Filters and Unscented Kalman Filters. Moving Horizon Estimation is considered when using nonlinear models or considering constraints on the estimates. Kalman Filters have been cited as being effective state estimators in cases of high model uncertainty and substantial noise (Rawlings et al., 2017; Vinodh et al., 2013). For the purposes of our work, a Kalman Filter is an appropriate choice due to the use of a linearized model of the system. The Kalman filter is used to estimate the state and disturbances from the converter's inductor current and output voltage measurements. This is to enable tracking of the reference voltage despite the presence of model mismatch or unmeasured nonzero mean disturbances (Pannocchia, 2015).

We start with an assumption that our system and measurements contain disturbances. The system model

becomes:

$$x[k+1] = Ax[k] + Bu + w \tag{3a}$$

$$y[k] = Cx[k] + v \tag{3b}$$

where $x[k]$ is the state variable, $u$ is the input and $y$ is the output (or measurement). $x[k+1]$ is the successor state. $w$ represents disturbances in the model, and hence, the state, while $v$ represents noise or inaccuracies in the measurement. $w$ has a normal distribution with 0 mean and variance $Q$, i.e. $w \sim N(0, Q)$. $v$ also has a 0 mean and variance $R$, i.e. $v \sim N(0, R)$. The larger the variance, the more uncertain we are about the parameter.

Kalman filters optimally estimate a system's state by fusing measurements with a state-space model of the system. The Kalman algorithm starts with a prediction step, in which the predicted state and predicted error covariance are evaluated using the system model and previously computed state estimate and error covariance values. The second step is the estimation (or correction) step in which the Kalman gain and error covariances are computed. Additionally, the state estimate is computed using the measured value and Kalman gain. Kalman gains are updated as new measurements are obtained.

The Kalman filter is added to the MPC controller to address load variations and their effect on the model. During load transients, the value of $R$, in the model changes. The disturbance estimator augments the math model of the boost converter with disturbances, i.e. we build a disturbance model. The disturbances introduced, $i_e$ and $v_e$ model the effect of the unmodelled load variations on the inductor current and output voltage respectively (Geyer et al., 2008; Karamanakos et al., 2013). The state variable is augmented with the disturbances as shown below in (4).

$$x_{aug}(t) = \begin{bmatrix} i_L(t) & v_o(t) & i_e(t) & v_e(t) \end{bmatrix}^T \tag{4}$$

An augmented model of the system is generated in (5). The model is used in the prediction step of the Kalman Filter (Karamanakos et al., 2013).

$$A_{ma} = \begin{bmatrix} A_m & \mathbf{0} \\ \mathbf{0} & \mathbf{I} \end{bmatrix} B_{ma} = \begin{bmatrix} B_m \\ \mathbf{0} \end{bmatrix} C = \begin{bmatrix} \mathbf{I} & \mathbf{I} \end{bmatrix} \tag{5}$$

The Kalman Filter then uses the model to estimate the augmented state variable in (6):

$$\hat{x}_{aug} = \hat{x}_{aug} + K_m(x - C\hat{x}_{aug}) \tag{6}$$

where $m$ in (5) and (6) represents the different modes in (2a) and can be selected from any value $\{1, 2, 3, 4\}$ depending on the switch position and amplitude of inductor current. $A_m$ and $B_m$ represent the state-space matrices of the original model in (2a) and are used in the augmented system model (5) to predict the state ($\hat{x}_{aug}$) and error covariance before measurement $x$. $K_m$ are the Kalman gains calculated for the different operating modes. $x$ is the measured state variable, while $\hat{x}_{aug}$ is the estimated state variable. **0** and **I** in are zero and identity matrices respectively.

The covariance value, $R$, is adjusted so that the Kalman filter ignores measurement errors by assigning a low value for $R$. This means that we have high confidence in our measurements and do not require compensation. However, a higher weight is assigned to the disturbance states in $Q$ in anticipation of process variability or model mismatches. The Kalman filter will estimate the disturbances $i_e$ and $v_e$, where $v_e$ will then be fed back to the MPC controller to compensate for the error by subtracting it from the reference.

## 4. Model predictive control

In the following sections, we describe time-triggered enumeration MPC followed by event-triggered MPC.

### 4.1. Time-triggered enumeration-based MPC

The MPC algorithm illustrated in Figure 1 starts with an evaluation of a set of switching sequences which are assembled over the prediction horizon. The number of prediction steps is represented with an integer number $N$. The duration of the prediction horizon is $NT_s$. The switching sequences are in the form $U(k) = [u(k), u(k+1) \ldots u(k+N-1)]^T$. Since the state of the switch is binary, the number of switching sequences totals to $2^N$. Due to the non-minimum phase behaviour of the boost converter, a longer prediction horizon is required to anticipate for the initial delay in response to the switch closing which requires an increase in $N$ since increasing $T_s$ would lead to an inaccuracy of math model which was developed using the Forward Euler Method. In an enumeration-based MPC, all switching sequences are evaluated by the controller, so every added switch state doubles the number of sequences to be evaluated which in turn increases the computational burden of the controller. To address this, a move blocking scheme is implemented (Karamanakos et al., 2013). Move blocking assigns the first number of switch steps $N_1$ with sample time $T_s$. The remaining steps $N_2$ are assigned a longer time sample by multiplying $T_s$ with a factor $n_s$. With a move blocking scheme, the total prediction horizon time is covered with fewer prediction steps.

The MPC solves an optimal control problem (OCP) (Boyd & Vandenberghe, 2004) for each switching

sequence, formulated as follows.

$$\min_{U_o} \quad \sum_{\ell=k}^{k+N-1} \left(|v_{o,err}(\ell+1|k)| + \lambda_u|\Delta u(\ell|k)| + \lambda_{i_L}|i_{L,err}(\ell|k)|\right) \tag{7a}$$

$$\text{s.t.} \quad \text{System dynamics (2)} \tag{7b}$$

In other words, the MPC controller predicts the future output voltage of the converter given a switch state within a sequence, and the measured input voltage, inductor current and output voltage at the time step. The absolute voltage error for the calculated output voltage ($v_{o,err}(k) = v_{ref} - v_o(k)$) and difference in switch state ($\Delta u(k) = u(k) - u(k-1)$) are then calculated for each switch state within the sequence. The weighing factor, $\lambda_u$, is applied to the difference between the two consecutive switching states to adjust the amount of switching, where increasing $\lambda_u$ generally reduces the switching frequency. $\lambda_{iL}$, is adjusted to control the influence of the inductor current error. The inductor current error is defined by: ($i_{L,err}(k) = i_{L,ref} - i_L(k)$), where, $i_{L,ref}$ is derived using the equation defined in (8):

$$v_s i_{L,ref} = R_L i_{L,ref}^2 + \frac{v_{ref}^2}{R} \tag{8}$$

Equation (8) represents the general power equation $P_{in} = P_{out}$, where the input power $P_{in}$, is equal to the inductor current $i_{L,ref}$ multiplied by the input voltage, $v_s$. As an estimate, we equate $P_{in}$ to the losses in the inductor series resistance, $R_L$, added to the power delivered to the load.

At each time step, the MPC controller evaluates the cost function (7a) for each of predefined switching sequences $U(k)$. In other words, for each of the $2^N$ sequences, the output voltage trajectory is predicted, and the objective function is evaluated. The switching sequence with minimum cost function value is then selected as the optimal switching sequence $U_o(k)$. The first element of the sequence is applied to the switch, $S$. This is referred to as a receding prediction horizon (Karamanakos et al., 2013). For time-triggered MPC, this procedure is repeated at the next time-step based on new measurements acquired at the following sampling instance. Feasibility is guaranteed since the MPC is solving an unconstrained optimization problem.

### 4.2. Event-triggered enumeration-based MPC

ET-MPC is introduced to reduce the computational burden of the enumeration TT-MPC. In TT-MPC, all $2^N$ switching sequences are evaluated at each time step $T_s$ which requires significant computational effort by the controller especially as the prediction steps $N$ increase. ET-MPC is proposed to solve the optimization problem only when an event is triggered, as opposed to solving at every time step. The algorithm starts with an event trigger which generates an optimal switching sequence $U_t[k]$ and optimal state trajectory $X_t[k]$. The first element in $U_t[k]$ is used to actuate the main switch $S$ and is fed back to the controller with a time delay. The controller also outputs the optimal switch sequence and state trajectory with a time delay along with counter $t$. Upon the next time step, the counter is incremented by $T_s$. The counter is used to increment index $k$ to select the next optimal switch state, but due to the move blocking scheme, index $k$ may need to be held for up to $n_s$ time samples. Index selection matrix $T$ is developed to address this. $T$ allocates counter $t$ to an equivalent index $k$ with consideration of the move blocking scheme. An example of $T$ is defined in Table 1. In this example $N = 6, N_1 = 4, n_s = 4$ and $Ts = 5\,\mu s$.

At the next time sample, given the optimal state sequence $X_{t1}$ computed at the last event (at time $t_1$), and the current output voltage measurement, $v_o$, an event-trigger $e$ is evaluated using the following criteria:

$$e = \begin{cases} 1 & \text{if } ||X_{t1}(2,k) - v_o|| > \delta \text{ or } k > k_{\max} \\ 0 & \text{Otherwise} \end{cases}, \tag{9}$$

where $\delta$ is defined as the trigger threshold and represents how much the output voltage deviates from the optimal state trajectory. An event is triggered when $e = 1$, which triggers the controller to evaluate the OCP. An event can also be triggered if $k_{\max}$ is reached which is the maximum allowable number of elements that can be used in the switching sequence. This generates a new optimal state trajectory and switching sequence which are fed back to the controller. Otherwise, when $e = 0$, the control action is determined using the next switch state in the optimal sequence $U_{t1}$ computed at the last event, which eliminates the need to run the optimization problem for the $2^N$ switching sequences (Chen & Yi, 2021). The event-triggered control algorithm is described in Algorithm 1. The cost function in Algorithm 1 is the argument of the OCP in (7a) and is defined as $J$. Figure 3 shows a block diagram of the proposed system.

## 5. Simulation results

The event-triggered Kalman-based MPC controller was implemented in MATLAB/SIMULINK. The parameters used in the simulation are listed in Table 2. The performance of the system is evaluated during start-up and step changes in the input voltage, reference voltage and load.

**Table 1.** Event-triggered selection of optimal state trajectory and switch state index.

| Counter $t$ | 5 µs | 10 µs | 15 µs | 20 µs | 25 µs | 30 µs | 35 µs | 40 µs | 45 µs | 50 µs | 55 µs | 60 µs |
|---|---|---|---|---|---|---|---|---|---|---|---|---|
| Index $k$ | 1 | 2 | 3 | 4 | | 5 | | | | 6 | | |
| $T[k]$ | 5 µs | 10 µs | 15 µs | 20 µs | | 40 µs | | | | 60 µs | | |
| $U_t[k]$ | $U_t[1]$ | $U_t[2]$ | $U_t[3]$ | $U_t[4]$ | | $U_t[5]$ | | | | $U_t[6]$ | | |
| $X[k]$ | $X[1]$ | $X[2]$ | $X[3]$ | $X[4]$ | | $X[5]$ | | | | $X[6]$ | | |

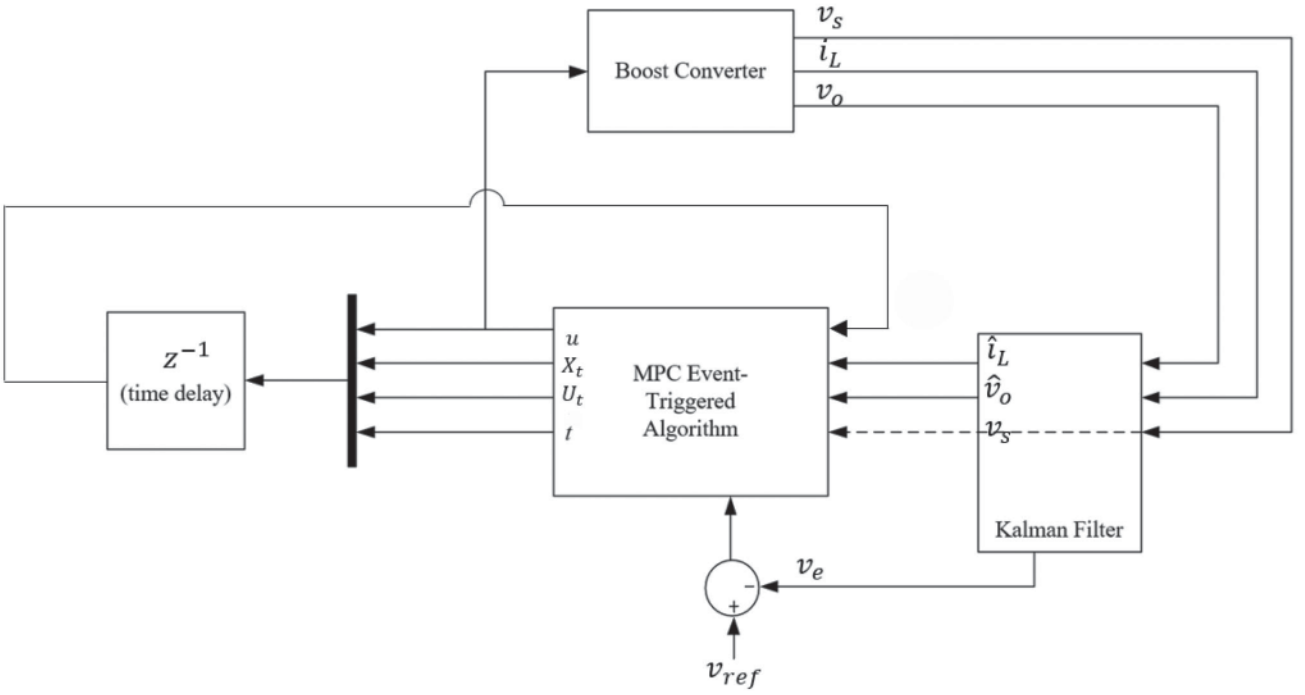


**Figure 3.** DC-DC boost converter with MPC control.

**Table 2.** Simulation parameters.

| Converter and controller parameter | Value |
|---|---|
| Input Voltage ($v_s$) | 15 V |
| Output Reference Voltage ($v_{ref}$) | 30 V |
| Inductor ($L$) | 450 µH |
| Inductor DC Resistance ($R_L$) | 0.8 Ω |
| Output Capacitance ($C$) | 220 µF |
| Load Resistance ($R$) | 73 Ω → 42 Ω |
| Sampling Period ($T_s$) | 5 µs |
| Prediction Horizon ($N$) | 14 |
| $N_1$ | 4 |
| Move Blocking Coefficient ($n_s$) | 4 |
| Allowable Optimal Switching Elements ($k_{max}$) | 6 |
| Switching – Weighing Factor ($\lambda_u$) | 0.35 |
| Inductor Current – Weighing Factor ($\lambda_{iL}$) | 0.1 |

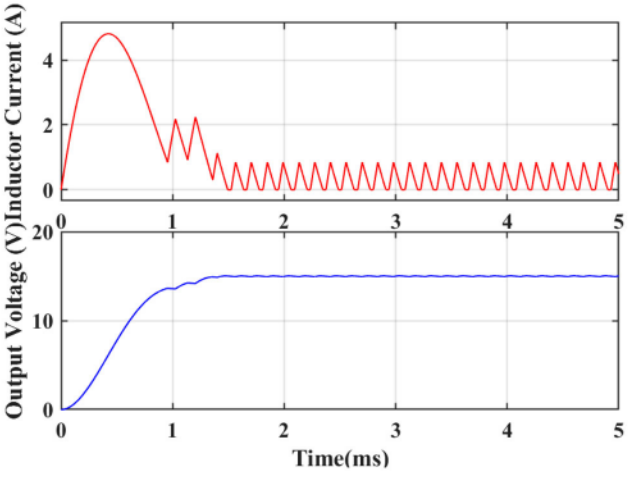


**Figure 4.** Start-up (TT-MPC).

### 5.1. Converter startup

The startup time of the converter was evaluated at different input voltages and output voltage references for both the time-triggered and event-triggered controllers. The results are listed in Table 3. The startup time is comparable for both implementations with no overshoot observed. The simulated inductor current and output voltage waveforms for the test case $Vin = 10$ V, $Vout = 15$ V are plotted in Figures 4 and 5. The event-trigger threshold of the MPC controller was set to $\delta = 0.025$. The number of event triggers are averaged using a moving average window of 200 and plotted.

During startup, switch $S$ remains in the open position allowing the output capacitor to charge and subsequently provide load current which causes an initial

**Algorithm 1** Event-Triggered MPC Algorithm

**procedure** ETMPC($u, U_{t1}, X_{t1}, t, i_L, v_o, v_s$)
  $J^*(k) = \infty$;
  $t \leftarrow t + T_s$
  $k \leftarrow$ select $k$ from $T$ using $t$ see Table 1
  $e \leftarrow$ compute (9);
  **if** $e = 1$ **then**
    $t \leftarrow 0$
    **for** all $U$ over $N$ **do**
      $J = 0$
      **for** $\ell = k$ to $k + N - 1$ **do**
        $x(\ell + 1) \leftarrow$ compute from (2), (4) and (5)
        $v_{o,err}(\ell + 1) = v_{ref} - v_o(\ell + 1)$
        $\Delta u(\ell) = u(\ell) - u(\ell - 1)$
        $v_{o,err}(\ell + 1) = v_{ref} - v_o(\ell + 1)$
        $J = J + |v_{o,err}(\ell + 1)|$
            $+\lambda_u|\Delta u(\ell)| + \lambda_{iL}\Delta i(\ell)$
      **end for**
      **if** $J < J^*(k)$ **then**
        $J^*(k) = J, u = U(1)$
      **end if**
    **end for**
    $U_t \leftarrow U$
    $X_t \leftarrow x$
  **else**
    $u \leftarrow U_{t1}(k)$
    $U_t \leftarrow U_{t1}$
    $X_t \leftarrow X_{t1}$
  **end if**
**return** $u, t, U_t, X_t$
**end procedure**

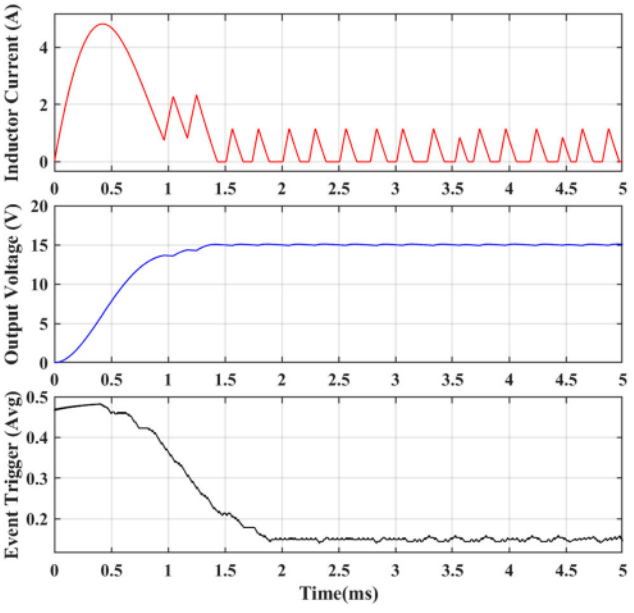


**Figure 5.** Start-up (ET-MPC).

**Table 3.** Start-up time summary.

| Operating conditions | Time-triggered MPC | Event-triggered MPC |
|---|---|---|
| $v_s = 10\,V, v_o = 15\,V$ | 1.4 ms | 1.4 ms |
| $v_s = 10\,V, v_o = 20\,V$ | 3.5 ms | 3.25 ms |
| $v_s = 10\,V, v_o = 25\,V$ | 7.3 ms | 7.5 ms |
| $v_s = 10\,V, v_o = 30\,V$ | 14.5 ms | 14.5 ms |
| $v_s = 15\,V, v_o = 20\,V$ | 1.5 ms | 1.5 ms |
| $v_s = 15\,V, v_o = 25\,V$ | 2 ms | 2 ms |
| $v_s = 15\,V, v_o = 30\,V$ | 3.75 ms | 3.75 ms |

inrush of current. The current is only limited by the inductor resistance $R_L$. Limiting this inrush current in this implementation cannot be done through the control of the switch, but can be achieved through external means such as employing a pre-charge resistor. After the output capacitor voltage equals the input voltage (neglecting the diode voltage drop), the voltage across the inductor becomes zero. At that point, the inductor current begins to drop and the voltage across the inductor reverses ($v_L = L(\mathrm{d}i/\mathrm{d}t)$) which allows the diode $D$ to remain forward biased and the output voltage to rise above the input voltage. However, the output voltage cannot be maintained in this manner due to the load demand and will begin to slightly drop, at this point, the controller will begin to actuate the switch $S$, and the converter will boost the output voltage to the voltage setpoint ($v_{ref}$).

Note that during the converter's initial operation, the event frequency is at its highest value (50%) due to the difference between output voltage and reference voltage Figure 5. Once the output voltage reaches the reference voltage in steady-state, the inductor current decreases. Once the converter reached Discontinuous Conduction Mode (DCM) operation, the event frequency significantly decreased (15%). In Badawi and Chen (2022b), it was found that the start-up time was mostly independent on the selection of the event-trigger threshold $\delta$ value, but was dependent on operating conditions.

The plots in Figure 6 show the gate signals, counter and instances of event triggers during steady-state operation when $v_{in} = 10\,V$ and $v_{ref} = 15\,V$. Since $k_{\max}$ is set to 6, $Ts = 5\,\mu s$ , $N_1 = 4$ and $n_s = 4$, the maximum counter value is calculated to be $60\,\mu s$ ($t_{\max} = N_1 T_s + n_s(k_{\max} - N_1)T_s$). In the actual implementation, we set the maximum counter value to $55\,\mu s$ . The optimal switching sequences in the time duration 4 and 5 ms are listed in Table 4. Any switching values with an index above 6 are discarded in the control. If we analyze the behaviour of the controller at time instance immediately before 4.3 ms. An event is triggered at that instant and the optimal switch sequence is found to be $U_t[k] = [0, 0, 0, 0, 0, 0]$. For the duration of $55\,\mu s$ , the sequence $U_t[k]$ is reused to actuate the main switch before triggering the next event due to reaching the maximum limit set for the counter $t$. The next event is triggered at 4.39 ms which still finds that

the same optimal switch state viable to maintain regulation, however, at 4.435 ms, the optimal switch sequence is updated to $U_t[k] = [1, 1, 1, 1, 1, 0]$.

### 5.2. Steady-state operation

The performance evaluation of the ET-MPC boost converter in Badawi and Chen (2022a, 2022b) in addition to our findings here, show that increasing the trigger threshold $\delta$ significantly reduces the computational effort of the controller during steady-state operation but that the tracking error, calculated using (10), increased. Increasing $\delta$ also increased the output voltage ripple and peak inductor current, and in some cases, the converter was not able to reach regulation, thus, putting a limit to our threshold selection.

$$T.E. = \sqrt{\frac{\sum_{i=1}^{n}(v_o[i] - v_{ref}[i])^2}{n}}. \tag{10}$$

The converter and controller parameters in this work slightly differ from what was reported in our previous work, and the threshold value is selected differently to achieve comparable results to a time-triggered controller. A comparison between TT-MPC and ET-MPC event frequency, tracking error and output ripple results are tabulated in Table 5. The computational savings are inferred from the event frequency. When events are not triggered, we are able to skip the optimization problem at each time step for up to $(N_1 + (k_{\max} - N_1)n_s)$ time steps. Additionally, when an event is not triggered, the MPC will only shift the index within the optimal control sequence and apply the actuating signal to switch $S$ without calculating the OCP. In a TT-MPC formulation, the number of operations per second (OPS) is calculated with equation (11):

$$OPS_{TT} = \frac{2^{N1+N2}}{T_s} \tag{11}$$

Here, each number of operations represents all the computations required to cycle through the optimization problem. The number of OPS in an ET-MPC can reach a minimum number given in (12). The assumption here is the optimal sequence is cycled through in its entirety and an event is only triggered when the counter reaches: $t_{\max} = N_1 T_s + n_s(k_{\max} - N_1)T_s$:

$$OPS_{ET} = \frac{2^{N1+N2}}{(N_1 + (k_{\max} - N_1)n_s)T_s} \tag{12}$$

The minimum event frequency is found using (13):

$$f_{\min -ET} = \frac{1}{(N_1 + (k_{\max} - N_1)n_s)} \tag{13}$$

By substituting the values in Table 2 in equation (13), we find that the minimum event frequency achievable is 1/12, or approximately 8.33%. The maximum computational savings per second can be found by substituting the parameters from Table 2 and the values found above in equation (14)

$$CS_{\max} = (1 - f_{\min -ET}) \times OPS_{TT} \tag{14}$$

As for our simulation results, the TT-MPC results are reported under $\delta = 0$. As the trigger threshold increases, the performance of the converter begins to degrade. Additionally, it was noted, that implementing an ET-MPC strategy results in reduced switching frequency from the TT-MPC formulation utilizing similar parameters. The switching frequency also reduces as the trigger-threshold is increased. Another observation is that the event frequency increases as the difference between the input and output voltage widens. A trade-off between the performance criteria and computational burden needs to be made when selecting the appropriate trigger-threshold (Badawi & Chen, 2022b).

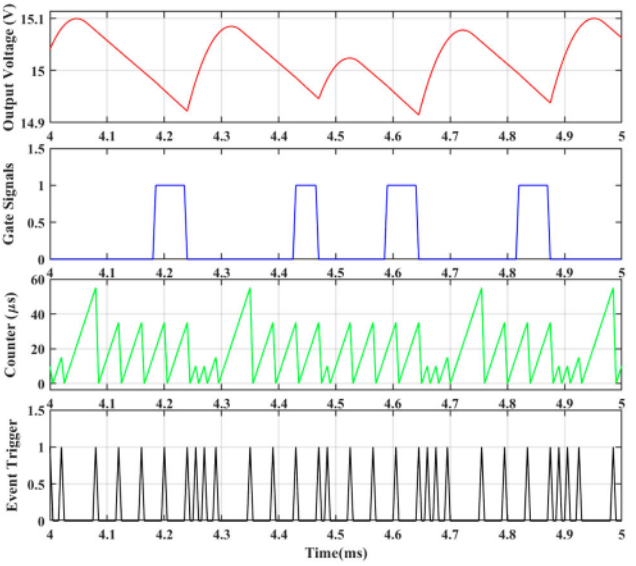


**Figure 6.** Steady-state (ET-MPC) $Vin = 10$ V, $V_{ref} = 15$ V.

**Table 4.** Optimal switching sequences in time duration between 4 ms and 5 ms in Figure 6.

| Time Duration | $U_t[1]$ | $U_t[2]$ | $U_t[3]$ | $U_t[4]$ | $U_t[5]$ | $U_t[6]$ |
|---|---|---|---|---|---|---|
| 4 ms → 4.165 ms | 0 | 0 | 0 | 0 | 0 | 0 |
| 4.165 ms → 4.205 ms | 0 | 1 | 1 | 1 | 1 | 0 |
| 4.205 ms → 4.245 ms | 1 | 1 | 1 | 1 | 0 | 0 |
| 4.245 ms → 4.435 ms | 0 | 0 | 0 | 0 | 0 | 0 |
| 4.435 ms → 4.475 ms | 1 | 1 | 1 | 1 | 1 | 0 |
| 4.475 ms → 4.57 ms | 0 | 0 | 0 | 0 | 0 | 0 |
| 4.57 ms → 4.61 ms | 0 | 1 | 1 | 1 | 1 | 0 |
| 4.61 ms → 4.65 ms | 1 | 1 | 1 | 1 | 0 | 0 |
| 4.65 ms → 4.8 ms | 0 | 0 | 0 | 0 | 0 | 0 |
| 4.8 ms → 4.84 ms | 0 | 1 | 1 | 1 | 1 | 0 |
| 4.84 ms → 5 ms | 0 | 0 | 0 | 0 | 0 | 0 |

**Table 5.** Event-trigger impact on steady-state operation – results summary.

| Steady-state conditions | $\delta = 0.00$ | $\delta = 0.01$ | $\delta = 0.015$ | $\delta = 0.025$ |
|---|---|---|---|---|
| | *Event frequency:* | | | |
| $v_s = 10\,V, v_o = 15\,V$ | 100% | 24.6% | 17.37% | 15% |
| $v_s = 10\,V, v_o = 20\,V$ | 100% | 34.7% | 25.6% | 17.3% |
| $v_s = 10\,V, v_o = 30\,V$ | 100% | 37.5% | 36% | 28.5% |
| $v_s = 15\,V, v_o = 30\,V$ | 100% | 34.4% | 32.8% | 23.8% |
| | *Tracking error [V]:* | | | |
| $v_s = 10\,V, v_o = 15\,V$ | 0.024 | 0.025 | 0.059 | 0.058 |
| $v_s = 10\,V, v_o = 20\,V$ | 0.03 | 0.03 | 0.035 | 0.06 |
| $v_s = 10\,V, v_o = 30\,V$ | 0.082 | 0.124 | 0.175 | 0.153 |
| $v_s = 15\,V, v_o = 30\,V$ | 0.081 | 0.113 | 0.113 | 0.146 |
| | *Output ripple [Vp-p]:* | | | |
| $v_s = 10\,V, v_o = 15\,V$ | 0.082 | 0.0945 | 0.1785 | 0.1854 |
| $v_s = 10\,V, v_o = 20\,V$ | 0.097 | 0.11 | 0.177 | 0.219 |
| $v_s = 10\,V, v_o = 30\,V$ | 0.134 | 0.24 | 0.273 | 0.31 |
| $v_s = 15\,V, v_o = 30\,V$ | 0.085 | 0.24 | 0.24 | 0.12 |

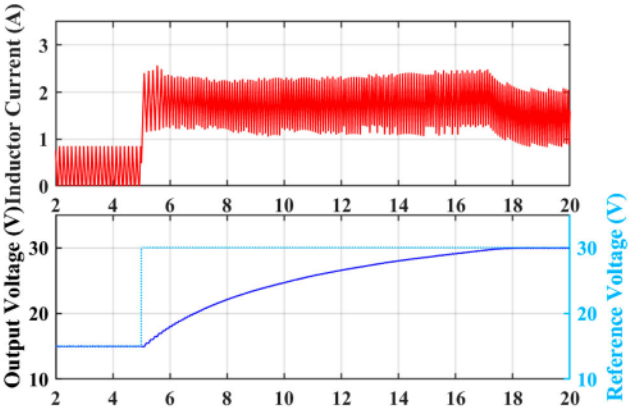


**Figure 7.** Reference voltage step-up from 15 to 30 V (Time-triggered MPC).

### 5.3. Step changes in the output reference voltage

Results were recorded while stepping up the output reference voltage from 15 V to 30. The input voltage was set to 10 V. The response time of the converter with different trigger thresholds was evaluated and recorded in Table 6. As observed from Figures 7 and 8, the output achieves a regulated 30 V within 13 ms for both TT-MPC and ET-MPC. During the transition, the event frequency, switching frequency and inductor current increase. The inductor current rms increases due to increase in load demand. Once the converter reaches regulation, the inductor current and event frequency are reduced. The transient time is similar for both time-triggered and event-triggered, and as noted above, utilizing the ET-MPC controller results in a reduced switching frequency for similar operating conditions experience when using the TT-MPC controller.

Figures 9 and 10 show simulation results when the voltage reference was stepped down from 25 to 15 V. Switch *S* remains OFF as the inductor current reduces to zero allowing the capacitor to discharge into the load to reduce the output voltage. The converter's regulation is

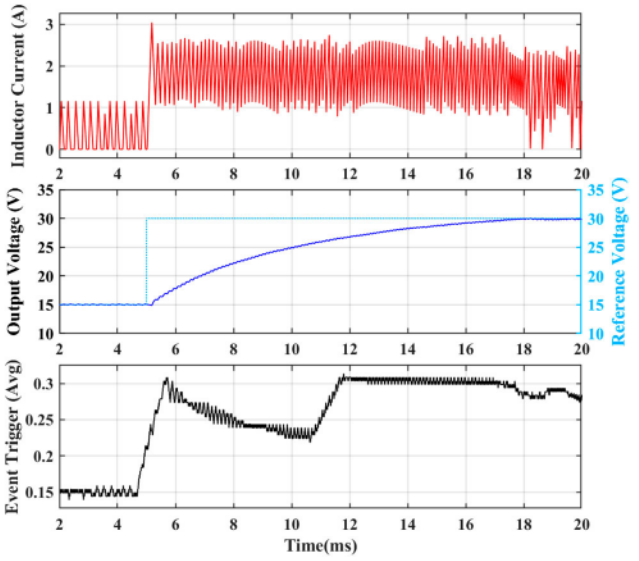


**Figure 8.** Reference voltage step-up from 15 to 30 V (Event-Triggered MPC).

almost equivalent for the two techniques, with the average number of computations significantly reduced with the latter method. The transient time was also similar for the two control techniques. The results for two different thresholds along with the TT-MPC implementation is summarized in Table 6.

**Table 6.** Voltage reference converter response for different event thresholds.

| | $\delta = 0.00$ | $\delta = 0.015$ | $\delta = 0.025$ |
|---|---|---|---|
| | $v_{ref} = 15\,V \rightarrow 30\,V, v_s = 10\,V$ | | |
| Transient time [ms] | 13 ms | 13 ms | 13 ms |
| Event Frequency | 100% | 40% | 30% |
| | $v_{ref} = 25\,V \rightarrow 15\,V, v_s = 10\,V$ | | |
| Transient time [ms] | 8 ms | 8 ms | 8 ms |
| Event Frequency | 100% | 25% | 13% |

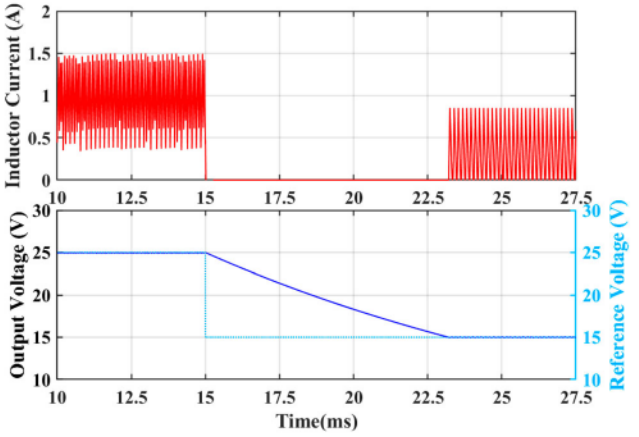


**Figure 9.** Reference voltage step-down from 25 to 15 V (Time-triggered MPC).

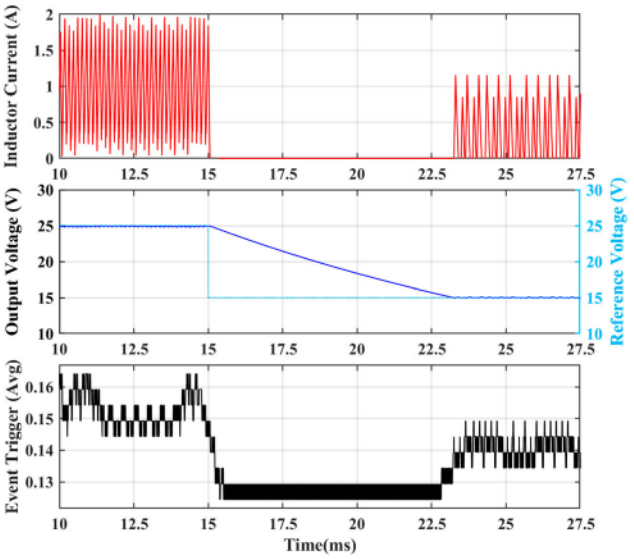


**Figure 10.** Reference voltage step-down from 25 to 15 V (Event-Triggered MPC).

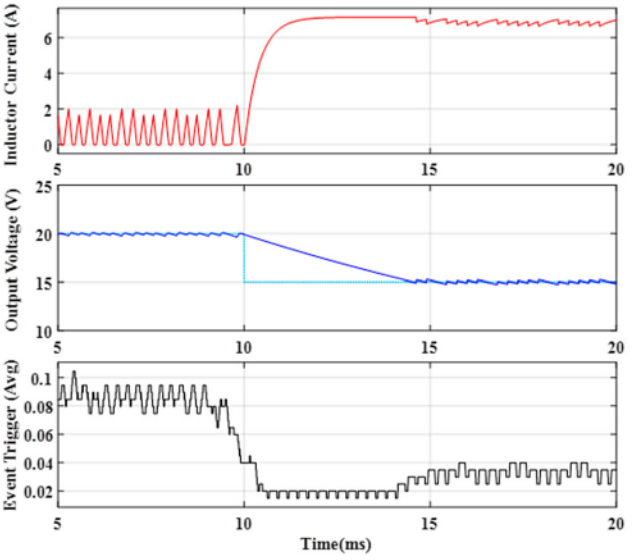


**Figure 11.** Inductor saturation (no current information in OCP).

One issue we had not accounted for originally in our work, prior to adding inductor current to the OCP (7a), was inductor saturation. Figure 11 shows the test result for when the reference voltage was stepped down from 20 to 15 V at 10 ms and $\delta = 0.005$. It was noted that without adding inductor information into the cost function, and in certain scenarios when the step down in reference voltage occurred as the inductor current was increasing (i.e. Switch *S* was *ON*), that the OCP would keep the switch *ON*, and only turn it to the *OFF* position to regulate the voltage. This is because the OCP found that to be the optimal solution. One quick remedy for the issue is to shift the step-down in reference voltage so that it coincides with a decrease in inductor current (i.e. switch *S* is in the *OFF* position) as observed in Figure 12. While this fixes the issue, it is not a practical solution. Figure 13 shows the same operating conditions with the inductor current added to the cost function which solved the issue with inductor saturation.

### 5.4. Step change in the input voltage

The ability of a converter to reject disturbances at the input source is a key requirement of any power converter controller. In Figures 14 and 15, the input voltage is stepped up from 10 to 15 V at 20 ms after steady state operation with $v_{ref}$ set to 30 V. The line transient response of the converter in both time-triggered and event-triggered formulations is similar showing that the converter is able to maintain the output voltage. The event frequency during the transient decreases by 6% as the difference between the input and output voltage decreases.

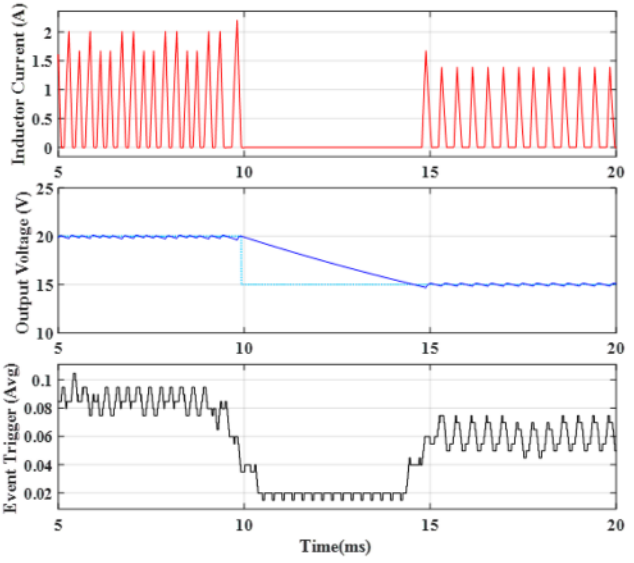


**Figure 12.** Inductor saturation addressed: shifted voltage reference from 10 to 9.92 ms.

### 5.5. Response to load transients

The load resistance *R* is reduced from 73 to 42Ω to simulate an increase in load demand. The change in load resistance is not captured in the MPC controller which results in inaccuracies of the control. Without compensating for the change in load, the output voltage will begin to sag

**Table 7.** Load transient results.

| | $\delta = 0.00$ | $\delta = 0.01$ | $\delta = 0.025$ |
|---|---|---|---|
| | $R = 73\,\Omega \rightarrow 42\,\Omega$ | | |
| Undershoot (V) | 0.3 V | 0.3 V | 0.3 V |
| Undershoot (%) | 1% | 1% | 1% |
| Settling time (ms) | 2 ms | 1.1 ms | 1 ms |

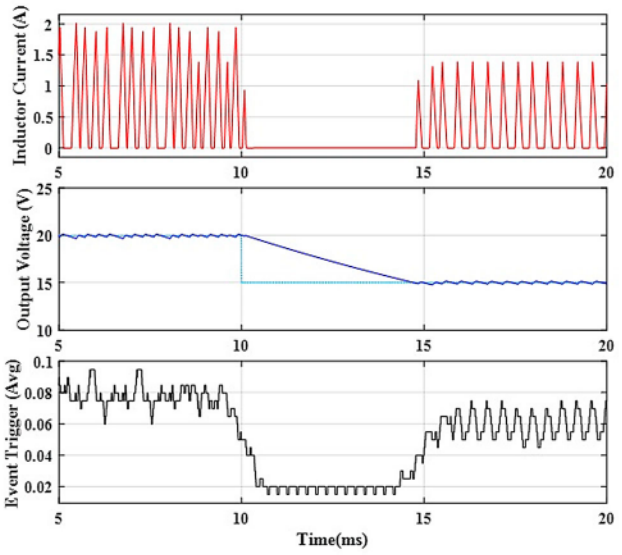


**Figure 13.** Inductor saturation addressed: add inductor current to OCP.

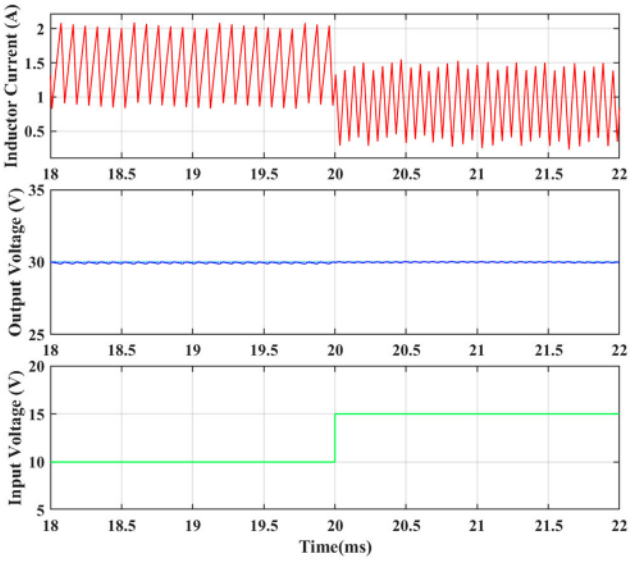


**Figure 14.** Input voltage step-up from 10 to 15 V (Time-triggered MPC).

and the controller will not able to regulate the converter to the reference voltage. The Kalman Filter is used to estimate the measured inductor current, output voltage and disturbance variables $i_e$ and $v_e$. The estimated voltage error is then subtracted from the voltage reference to adjust for disturbances in the load.

The output reference voltage is set to 30 V and input voltage set to 15 V. The covariance matrices for process noise, $Q$, and measurement noise, $R$, are assigned the values in (15) :

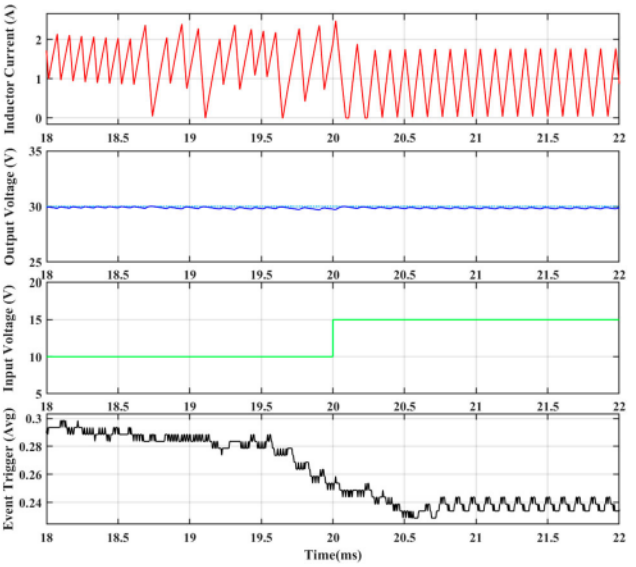


**Figure 15.** Input voltage step-up from 10 to 15 V (Event-Triggered MCP).

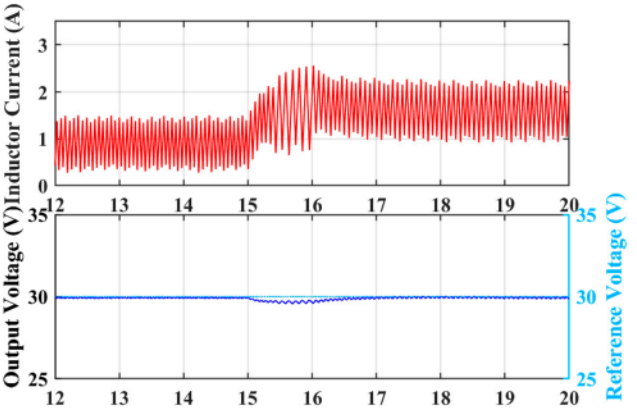


**Figure 16.** Load transient for time-triggered MPC.

$$Q = \begin{bmatrix} 0.1 & 0 & 0 & 0 \\ 0 & 0.1 & 0 & 0 \\ 0 & 0 & 50 & 0 \\ 0 & 0 & 0 & 50 \end{bmatrix} \quad R = \begin{bmatrix} 1 & 0 \\ 0 & 1 \end{bmatrix} \qquad (15)$$

The time-triggered simulated waveform is shown in Figure 16. The undershoot measured 0.3 V which is equivalent to 1% of the reference voltage. The settling time for the transient was 2 ms and the converter was able to return to regulation.

The output voltage when a load transient was applied to the converter using ET-MPC control with $\delta$ set to 0.01 is shown in Figure 17. The undershoot was 1%; similar with the TT-MPC result, but with a faster settling time 1.1 ms. When the threshold was set to $\delta = 0.025$ the voltage was able to return to regulation within 1 ms; the undershoot was also 1% Figure 18. The aforementioned results are tabulated in Table 7. The results show that ET-MPC

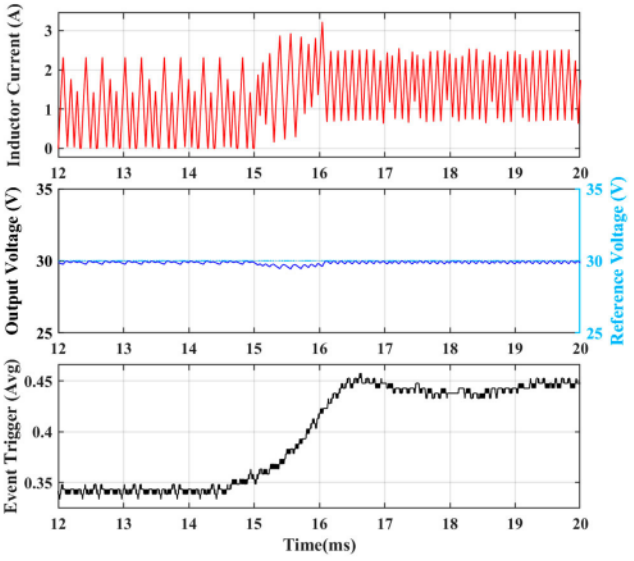


**Figure 17.** Load transient for ET-MPC, $\delta = 0.01$.

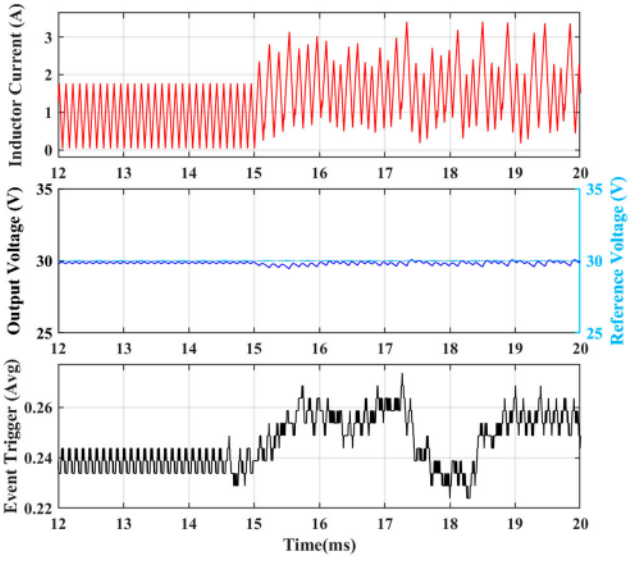


**Figure 18.** Load transient for ET-MPC, $\delta = 0.025$.

can reduce the overall computational burden of TT-MPC, but the trade-off being higher peak inductor current and output voltage ripple.

## 6. Remarks

There are several parameters that impact the performance of our boost converter ET-MPC controller. The influence of the trigger threshold, $\delta$, was briefly evaluated in this work while its selection criteria and performance impact was extensively explored in Badawi and Chen (2022b). Generally, increasing the trigger threshold reduces the computational burden, but increa ses tracking error, output ripple and peak inductor current. Additional parameters include the switching weighing factor $\lambda_u$ which penalizes switching and can be used to control the switching frequency. The inductor current weighing factor $\lambda_{i_L}$, described in Section 4, penalizes the error between the inductor reference and measured inductor current. Increasing this value increases the tightness of current control and prevents inductor saturation but excessively increasing this value can cause the controller to lose voltage regulation. Another factor is $k_{\max}$ in (9), which is the maximum allowable number of elements that can be used in the switching sequence. Reducing this number improves the performance of the control but increases the computational burden as more events are triggered.

The effect of changing these values was not evaluated explicitly here. We leave the evaluation of these parameters for later work.

## 7. Conclusion

This work introduces an effective method to reduce the computational burden associated with a finite control set enumeration-based model predictive control (MPC) used for the direct control of a DC-DC converter. Simulation results demonstrate that the performance of the proposed event-triggered MPC is comparable with the conventional time-triggered MPC while achieving reduction in the computational burden of the controller. A similar approach can be implemented on different converters such as buck converters, with minimum modification. Future work includes an analytical study on the optimality loss of the proposed event-triggered MPC and the application to a buck converter. Implementation of the proposed control algorithms in hardware to verify the stability of real-time implementation will be considered for future work.

## Acknowledgments

Ranya Badawi: Data curation, Formal analysis, Investigation, Methodology, Writing-original draft, review & editing, Investigation, Software and Validation. Jun Chen: Conceptualization, Methodology, Investigation, Funding acquisition, Writing-review and editing, and Supervision. Both authors have read and approved the final version of the manuscript.

## Disclosure statement

No potential conflict of interest was reported by the author(s).

## Funding

This work was supported in part by the faculty startup fund from Oakland University and in part by National Science Foundation through Award #2237317. (*Jun Chen is the corresponding author.*)

## Data availability statement

The authors agree to make available data and materials supporting the results and analyses upon request.

## References


Ahmed, M., Abdelrahem, M., Kennel, R., & Hackl, C. M. (2020a). A robust maximum power point tracking based model predictive control and extended Kalman filter for PV systems. In *2020 International symposium on power electronics, electrical drives, automation and motion (SPEEDAM)* (pp. 514–519).

Ahmed, M., Abdelrahem, M., Kennel, R., & Hackl, C. M. (2020b). Maximum power point tracking based model predictive control and extended Kalman filter using single voltage sensor for PV systems. In *2020 IEEE 29th international symposium on industrial electronics (ISIE)* (pp. 1039–1044).

Badawi, R., & Chen, J. (2022a, July 12–15). Enhancing enumera tion-based model predictive control for DC-DC boost converter with event-triggered control. In *European control conference*, London, UK.

Badawi, R., & Chen, J. (2022b). Performance evaluation of event-triggered model predictive control for boost converter. In *2022 IEEE vehicle power and propulsion conference (VPPC)* (pp. 1–6).

Beccuti, A. G., Mariethoz, S., Cliquennois, S., Wang, S., & Morari, M. (2009). Explicit model predictive control of DC–DC switched-mode power supplies with extended Kalman filtering. *IEEE Transactions on Industrial Electronics*, *56*(6), 1864–1874. https://doi.org/10.1109/TIE.2009.2015748

Boyd, S. P., & Vandenberghe, L. (2004). *Convex optimization*. Cambridge University Press.

Chen, J., Behal, A., & Li, C. (2021, December 13–15). Active cell balancing by model predictive control for real time range extension. In *2021 IEEE conference on decision and control*, Austin, TX, USA.

Chen, J., Li, Z., & Yin, X. (2021, April 7–9). Optimization of energy storage size and operation for renewable-EV hybrid energy systems. In *2021 IEEE green technologies conference*, Denver, CO.

Chen, J., Liang, M., & Ma, X. (2021, April 7–9). Probabilistic analysis of electric vehicle energy consumption using MPC speed control and nonlinear battery model. In *2021 IEEE green technologies conference*, Denver, CO.

Chen, J., Meng, X., & Li, Z. (2022, June 8–10). Reinforcement learning-based event-triggered model predictive control for autonomous vehicle path following. In *American control conference*, Atlanta, GA.

Chen, Q., Wang, B., Peng, W., & Rodriguez, J. (2021). Cost function decoupling of FS-MPC for power converter using event-triggered mechanism. In *2021 IEEE international conference on predictive control of electrical drives and power electronics (PRECEDE)* (pp. 104–108). IEEE.

Chen, L., Xu, Y., & Heng, N. (2019). Improved finite set model predictive current control of grid side converter in weak grid using Kalman filter. In *2019 IEEE PES asia-pacific power and energy engineering conference (APPEEC)* (pp. 1–5).

Chen, J., & Yi, Z. (2021, Aug. 8–11). Comparison of event-triggered model predictive control for autonomous vehicle path tracking. In *IEEE conf. control technology and applications*, San Diego, CA.

Cortes, P., Kouro, S., La Rocca, B., Vargas, R., Rodriguez, J., Leon, J. I., Vazquez, S., & Franquelo, L. G. (2009). Guidelines for weighting factors design in model predictive control of power converters and drives. In *2009 IEEE International Conference on Industrial Technology* (pp. 1–7).

Ding, W., Faraji, F., Jayan, V., Zuo, W., Ghias, A. M., & Cha, H. (2022). Finite control set model predictive control for five-level modified active nested neutral point clamped converter. In *2022 IEEE energy conversion congress and exposition (ECCE)* (pp. 1–5). IEEE.

Di Salvo, S. R., Leuzzi, R., Tresca, G., Anglani, N., & Zanchetta, P. (2022). Self-tuning finite-state model predictive control with grid impedance estimation in a grid-tied inverter. In *2022 IEEE energy conversion congress and exposition (ECCE)* (pp. 1–7). IEEE.

Eqtami, A., Dimarogonas, D. V., & Kyriakopoulos, K. J. (2011, December 12–15). Novel event-triggered strategies for model predictive controllers. In *2011 50th IEEE conference on decision and control and european control conference* (pp. 3392–3397), Orlando, FL.

Erickson, R. W., & Maksimovic, D. (2007). *Fundamentals of power electronics*. Springer Science & Business Media.

Gardezi, M. S. M., & Hasan, A. (2018). Machine learning based adaptive prediction horizon in finite control set model predictive control. *IEEE Access*, *6*, 32 392–32 400. https://doi.org/10.1109/ACCESS.2018.2839519

Geyer, T., Papafotiou, G., Frasca, R., & Morari, M. (2008). Constrained optimal control of the step-down DC–DC converter. *IEEE Transactions on Power Electronics*, *23*(5), 2454–2464. https://doi.org/10.1109/TPEL.2008.2002057

Han, M., He, H., Wang, X., Dong, Z., & Zhang, Z. (2021). Current-sensorless model predictive control of dual active bridge converters with Kalman filter. In *2021 IEEE international conference on predictive control of electrical drives and power electronics (PRECEDE)* (pp. 663–667).

Hargrave, P. (1989). A tutorial introduction to Kalman filtering. In *IEE colloquium on Kalman filters: introduction, applications and future developments* (pp. 1–1). IET.

Hashimoto, K., Adachi, S., & Dimarogonas, D. V. (2016). Self-triggered model predictive control for nonlinear input-affine dynamical systems via adaptive control samples selection. *IEEE Transactions on Automatic Control*, *62*(1), 177–189. https://doi.org/10.1109/TAC.2016.2537741

Jin, S., Zhuo, S., & Huangfu, Y. (2022). Offset-free model predictive control of interleaved boost converter based on extended state observer. In *2022 4th International conference on smart power & internet energy systems (SPIES)* (pp. 268–273).

Karamanakos, P., & Geyer, T. (2020). Guidelines for the design of finite control set model predictive controllers. *IEEE Transactions on Power Electronics*, *35*(7), 7434–7450. https://doi.org/10.1109/TPEL.63

Karamanakos, P., Geyer, T., & Manias, S. (2013). Direct voltage control of DC–DC boost converters using enumeration-based model predictive control. *IEEE Transactions on Power Electronics*, *29*(2), 968–978. https://doi.org/10.1109/TPEL.2013.2256370

Karamanakos, P., Liegmann, E., Geyer, T., & Kennel, R. (2020). Model predictive control of power electronic systems: Methods, results, and challenges. *IEEE Open Journal of Industry Applications*, *1*, 95–114. https://doi.org/10.1109/OJIA

Kouro, S., Cortés, P., Vargas, R., Ammann, U., & Rodríguez, J. (2008). Model predictive control – A simple and powerful

method to control power converters. *IEEE Transactions on Industrial Electronics*, *56*(6), 1826–1838. https://doi.org/10.1109/TIE.2008.2008349

Li, H., & Shi, Y. (2014). Event-triggered robust model predictive control of continuous-time nonlinear systems. *Automatica*, *50*(5), 1507–1513. https://doi.org/10.1016/j.automatica.2014.03.015

Liang, C., Dong, Z., Zhang, Q., Cao, T., Gao, X., Wang, N., & Zhang, Z. (2023). Event-triggered MPC for current-source-mode single-inductor multiple-port DC-DC converter. In *2023 IEEE 14th international symposium on power electronics for distributed generation systems (PEDG)* (pp. 932–937). IEEE.

Liang, Y., Liang, Z., Zhao, D., Huangfu, Y., & Guo, L. (2018). Model predictive control for interleaved DC-DC boost converter based on Kalman compensation. In *2018 IEEE international power electronics and application conference and exposition (PEAC)* (pp. 1–5).

Liang, Y., Liang, Z., Zhao, D., Huangfu, Y., Guo, L., & Zhao, B. (2019). Model predictive control of interleaved DC-DC boost converter with current compensation. In *2019 IEEE international conference on industrial technology (ICIT)* (pp. 1701–1706).

Lin, H., Liu, J., Shen, X., Yin, Y., Leon, J. I., Franquelo, L. G., & Wu, L. (2021). Event-triggered continuous control set-model predictive control for three-phase power converters. In *IECON 2021–47th annual conference of the IEEE Industrial Electronics Society* (pp. 1–6). IEEE.

Liu, X., Qiu, L., Wu, W., Ma, J., Fang, Y., Peng, Z., Wang, D., & Rodríguez, J. (2022). Event-triggered ESO-based robust MPC for power converters. *IEEE Transactions on Industrial Electronics*, *70*(2), 2144–2152. https://doi.org/10.1109/TIE.2022.3167135

Pannocchia, G. (2015). Offset-free tracking MPC: A tutorial review and comparison of different formulations. In *2015 European control conference (ECC)* (pp. 527–532). IEEE.

Pannocchia, G., & Bemporad, A. (2007). Combined design of disturbance model and observer for offset-free model predictive control. *IEEE Transactions on Automatic Control*, *52*(6), 1048–1053. https://doi.org/10.1109/TAC.2007.899096

Rathore, N., & Fulwani, D. (2016). Event triggered control scheme for power converters. In *IECON 2016-42nd annual conference of the IEEE Industrial Electronics Society* (pp. 1342–1347). IEEE.

Rawlings, J. B., Mayne, D. Q., & Diehl, M. (2017). *Model predictive control: Theory, computation, and design* (Vol. 2). Nob Hill Publishing.

Rigatos, G., Busawon, K., Siano, P., & Abbaszadeh, M. (2018). A Kalman filter-based disturbance observer for state-of-charge estimation in EV batteries. In *2018 AEIT international annual conference* (pp. 1–6). IEEE.

Rodriguez, J., & Cortes, P. (2012). *Predictive control of power converters and electrical drives*. Wiley.

Serri, E., & Ahmad, A. Z. (2016). Comparative study of short prediction MPC-KF with PI controller for DC-DC buck converter. In *2016 IEEE international conference on automatic control and intelligent systems (I2CACIS)* (pp. 219–224).

Snehal, N., Pooja, W., & Sonam, K. (2021). Model predictive control for DC-DC buck converter using enumeration. In *2020 52nd North American power symposium (NAPS)* (pp. 1–6).

Umeno, N., & Maruta, H. (2020). Stabilization improvement of MPC based DC-DC converter with load estimation. In *2020 9th International conference on renewable energy research and application (ICRERA)* (pp. 295–300). IEEE.

Villarroel, F. A., Espinoza, J. R., Pérez, M. A., Ramírez, R. O., Baier, C. R., Sbárbaro, D., Silva, J. J., & Reyes, M. A. (2021). Stable shortest horizon FCS-MPC output voltage control in non-minimum phase boost-type converters based on input-state linearization. *IEEE Transactions on Energy Conversion*, *36*(2), 1378–1391. https://doi.org/10.1109/TEC.60

Vinodh, K. E., Jovitha, J., & Ayyappan, S. (2013). Comparison of four state observer design algorithms for MIMO system. *Archives of Control Sciences*, *23*(2), 131–144. https://doi.org/10.2478/acsc-2013-0015

Wang, B., Huang, J., Wen, C., Rodriguez, J., Garcia, C., Gooi, H. B., & Zeng, Z. (2020). Event-triggered model predictive control for power converters. *IEEE Transactions on Industrial Electronics*, *68*(1), 715–720. https://doi.org/10.1109/TIE.41

Xie, Y., Ghaemi, R., Sun, J., & Freudenberg, J. S. (2009). Implicit model predictive control of a full bridge dc–dc converter. *IEEE Transactions on Power Electronics*, *24*(12), 2704–2713. https://doi.org/10.1109/TPEL.2009.2030196

Yoo, J., & Johansson, K. H. (2021). Event-triggered model predictive control with a statistical learning. *IEEE Transactions on Systems, Man, and Cybernetics: Systems*, *51*(4), 2571–2581. https://doi.org/10.1109/TSMC.2019.2916626